Decoupling of rainfall and vegetation greening in the arid Asian endorheic basins due to the irrigation intensification

Zhengyang Zhang[1], Xuanlong Ma[1], Eduardo Eiji Meada[2], Lei Lu[3], Yuanyuan Wang[4], Zunyi Xie[5], Xiaoying Li[6], Lei Huang[7], Yuhe Zhao[8], and Alfredo R Huete[9]

[1]Lanzhou University
[2]Department of Geosciences and Geography, P.O. Box 68, FI-00014 University of Helsinki, Finland.
[3]College of Earth and Environmental Sciences, Lanzhou University
[4]Key Laboratory of Radiometric Calibration and Validation for Environmental SatellitesNational Satellite Meteorological Center (National Center for Space Weather)China Meteorological Administration, Beijing 100082, China.
[5]Henan University
[6]College of Earth and Environmental Sciences, Lanzhou University, Lanzhou, Gansu, 730000 China
[7]Institute of Remote Sensing and Digital Earth, Chinese Academy of Sciences
[8]College of Earth and Environmental Sciences, Lanzhou University, Lanzhou, Gansu, 730000 China.
[9]University of Technology Sydney

May 13, 2023

Abstract

A large portion of Central-Western Asia is made up of contiguous closed basins, collectively termed as the Asian Endorheic Basins (AEB). As these retention basins are only being replenished by the intermittent precipitation, increasing droughts in the region and a growing demand for water have been presumed to jointly contributed to the land degradation. To understand the impact of climate change and human activities on dryland vegetation over the AEB, we conducted trend and partial correlation analysis of vegetation and hydroclimatic change from 2001 to 2021 using multi-satellite observations, including vegetation greenness, total water storage anomalies (TWSA) and meteorological data. Here we show that much of the AEB (65.53%) exhibited a greening trend over the past two decades. Partial correlation analyses indicated that climatic factors had varying effects on vegetation productivity as a function of vegetation types and aridity. In arid AEB, precipitation dominated the vegetation productivity trend. Such a rainfall dominance gave way to TWSA dominance in the hyper-arid AEB. We further showed that the decoupling of rainfall and hyper-arid vegetation greening was largely due to a significant expansion (17.3%) in irrigated cropland across the hyper-arid AEB. Given the extremely harsh environment in the hyper-arid AEB, our results therefore raised the concerns on the ecological and societal sustainability in this region, where a mild increase in precipitation might not be able to catch up the rising evaporative demand and water consumption resulted from global warming and irrigation intensification.

Hosted file

961761_0_art_file_10924709_rj4mcd.docx available at https://authorea.com/users/561506/articles/642448-decoupling-of-rainfall-and-vegetation-greening-in-the-arid-asian-

endorheic-basins-due-to-the-irrigation-intensification

Decoupling of rainfall and vegetation greening in the arid Asian endorheic basins due to the irrigation intensification

Zhengyang Zhang[1], Xuanlong Ma[1*], Eduardo Eiji Maeda[2, 3], Lei Lu[1], Yuanyuan Wang[4, 5], Zunyi Xie[6], Xiaoying Li[1], Lei Huang[7], Yuhe Zhao[1], and Alfredo Huete[8]

[1]College of Earth and Environmental Sciences, Lanzhou University, Lanzhou, Gansu, 730000 China.

[2]Department of Geosciences and Geography, P.O. Box 68, FI-00014 University of Helsinki, Finland.

[3]Finnish Meteorological Institute, FMI, Helsinki, Finland.

[4]Key Laboratory of Radiometric Calibration and Validation for Environmental Satellites，National Satellite Meteorological Center（National Center for Space Weather），China Meteorological Administration, Beijing 100082, China.

[5]Innovation Center for FengYun Meteorological Satellite (FYSIC), Beijing 100082, China.

[6]Centre for Biodiversity and Conservation Science, School of Earth and Environmental Sciences, The University of Queensland, Brisbane, QLD, Australia.

[7]Aerospace Information Research Institute, Chinese Academy of Sciences, Beijing, 100094, China.

[8]Faculty of Science, University of Technology Sydney, Sydney, NSW 2007, Australia

Corresponding author: Xuanlong Ma (xlma@lzu.edu.cn)

Key Points:

- An overall greening trend was found in the AEB expecially in Northwest China, Qinghai Tibet Plateau, and Western Asia during 2001-2021.
- Precipitation had the dominant control effect in arid zones, vegetation change in hyper-arid zones was most closely associated with TWSA.
- A significant expansion of irrigated cropland (agricultural development) in hyper-arid zones was positively correlated with greening.

Abstract

A large portion of Central-Western Asia is made up of contiguous closed basins, collectively termed as the Asian Endorheic Basins (AEB). As these retention basins are only being replenished by the intermittent precipitation, increasing droughts in the region and a growing demand for water have been presumed to jointly contributed to the land degradation. To understand the impact of climate change and human activities on dryland vegetation over the AEB, we conducted trend and partial correlation analysis of vegetation and hydroclimatic change from 2001 to 2021 using multi-satellite observations, including vegetation greenness, total water storage anomalies (TWSA) and meteorological data. Here we show that much of the AEB (65.53%) exhibited a greening trend over the past two decades. Partial correlation analyses indicated that climatic factors had varying effects on vegetation productivity as a function of vegetation types and aridity. In arid AEB, precipitation dominated the vegetation productivity trend. Such a rainfall dominance gave way to TWSA dominance in the hyper-arid AEB. We further showed that the decoupling of rainfall and hyper-arid vegetation greening was largely due to a significant expansion (17.3%) in irrigated cropland across the hyper-arid AEB. Given the extremely harsh environment in the hyper-arid AEB, our results therefore raised the concerns on the ecological and societal sustainability in this region, where a mild increase in precipitation might not be able to catch up the rising evaporative demand and water consumption resulted from global warming and irrigation intensification.

Plain Language Summary

Asian Endorheic Basins (AEB), including Central Asia, Caspian Sea, Mongolia Plateau, Northwest China, Qinghai Tibet Plateau, and Western Asia, are typical drylands that have fragile ecosystems. Increased water demand from agricultural expansion have been presumed to jointly contributed to the land degradation over the AEB. Here we analyzed the vegetation greening pattern and the relationship with hydroclimatic driving factors and land use change. Results showed that much of the AEB exhibited a greening trend over the past two decades. We also found that the hyper-arid vegetation greening was largely due to the irrigation intensification, leading to the overexploitation of groundwater signified by an alarming rate of persistent decline in groundwater. This paper offers valuable insight into the ecological responses to climate and human activities in the AEB and can hence guide large-scale sustainable development plans to address the challenges of future climate change in an extremely vulnerable environment.

1 Introduction

Drylands cover approximately 41% of the Earth's land surface and are commonly characterized by scarce water resources (Smith et al., 2019). Dryland vegetation forms a vital component that provides essential services to the terrestrial ecosystem, and supports biodiversity, livelihoods, and food production (Riis et al., 2020; Ukkola et al., 2021). The Asian Endorheic Basins (AEB) scattered across Central Asia, Caspian Sea, Mongolia Plateau, Northwest China, Qinghai Tibet Plateau, and Western Asia, are emblematic arid and semi-arid dryland ecosystems. These basins retain water, but are replenished intermittently, thus making the ecosystems vulnerable to extreme climate events (Jiao et al., 2021; Li et al., 2015; Pan et al., 2019). In addition, the population of the AEB has exploded over the last ten years, and these regions are thought to house nearly 278 million people (3.6% of the global population) (CIESIN, 2018).

Climate change coupled with the increasing demand for water and other resources by people threatens the ecological and social sustainability of the AEB (Safriel et al., 2008). Consequently, disentangling the impact of climate change on vegetation in the AEB is of great importance for regional sustainable development (Liu et al., 2018; Wei et al., 2021).

A large proportion of bare land and limited water resources make the AEB prone to land degradation and desertification. Studies on global vegetation dynamics suggest that vegetation change in the Anthropocene shows a high degree of spatial heterogeneity and varies greatly across different ecosystems, which makes challenges in global change prediction (Mander et al., 2017; Xing et al., 2022; Zeng et al., 2021). In Northwest China, the eastern section of the AEB, vegetation showed a greening trend since 1982 (Jiang et al., 2018). The greening trend was mainly found in mountainous areas and oases, while the shrublands, grasslands, and deserts experienced degradation (Wang et al., 2021; Liang et al., 2020). In Central Asia, the middle section of the AEB, studies revealed a significant greening trend from 1982 to 1994, but then turned to be brown afterward (Luo et al., 2020; Yin et al., 2016). Similar to Northwest China, the browning trend in Central Asia was mainly in deserts and grassland (Xing et al., 2022; Yuan et al., 2021).

However, spatially heterogeneous process of greening and browning and poorly understanding of a suite of hydroclimatic factors make it be challenging to predict the influence of the climate in future years (Na et al., 2021; Piao et al., 2020). Precipitation has been recognized as the major factor that regulates vegetation growth in drylands (Liu et al., 2021; Yang et al., 2021), but temperature also plays a role as it affects water availability by altering the atmospheric water demand via the potential evapotranspiration (Nagler et al., 2007). Recent studies have suggested that geohydrological factors such as Terrestrial Water Storage (TWS) can also affect dryland vegetation productivity (Seka et al., 2022; Zhang et al., 2022), in some cases, the relative importance of TWS may even surpass precipitation (e.g., Yang et al., Cao et al. 2022). To further complicate the ability to predict vegetation change, human activities including farming, infrastructure construction, and industrial water consumption can have different impacts on vegetation (Chen et al., 2020; Li et al., 2022a).

The intersection of these factors means that predicting and modeling ecosystem change can be extremely challenging, particularly across an area as spatially heterogeneous as the EEB (Mohamed et al., 2018). Therefore, it is expected to capture the spatially explicit characterization of the trend in vegetation productivity with consideration of not only precipitation and temperature but also water storage and human activity. To address this issue, we have employed the highly-calibrated MODIS data spanning the last two decades to examine changes in vegetation productivity with the development of this region. Instead of using the potentially outdated GIMMS NDVI3g dataset in most modeling efforts for the region, we use the MODIS data, hoping to not only characterize the spatial patterns of change in the EEB, but also to identify generalizable spatial patterns and provide insight into the underlying mechanisms that dictate varying sensitivities of the ecosystem to hydroclimatic change.

The overarching aim of this study is to quantify changes in vegetation productivity within the EEB over the past two decades, and to identify any hydroclimatic factor that appears to drive or predict this change. Specifically, our objectives are to 1) characterize the temporal trend of integrated MODIS EVI (IntEVI), a satellite proxy of vegetation productivity, in growing season from 2001 to 2021 over the EEB; 2) quantify the driving factors of the IntEVI trend at each pixel including precipitation, temperature, and terrestrial water storage; and to 3) generalize the

relative role of hydroclimatic condition and vegetation types on the relationships between vegetation productivity and hydroclimatic factors across these endorheic dryland ecosystems.

2 Materials and Methods

2.1 Study Area

The Asian endorheic basins (AEB) are located in the Asian inland, which is commonly divided into six major geographic units: Central Asia (CA), Caspian Sea (CS), Mongolia Plateau (MGP), Northwest China (NC), Qinghai Tibet Plateau (QTP), and Western Asia (WA) (Fig. 1). The entire AEB spans from the latitude of 34.43°E to 119.98°E and the longitude of 13.92°N to 56.24°N, with a total area of 1.34×107 km^2, and is known to be one of the most ecologically fragile regions in the world (Yu et al., 2016; Huang et al., 2016; Mu et al., 2021). In this region, the average annual temperature ranges from -19°C to 27°C, and the total annual precipitation varies between less than 50 mm to more than 800 mm.

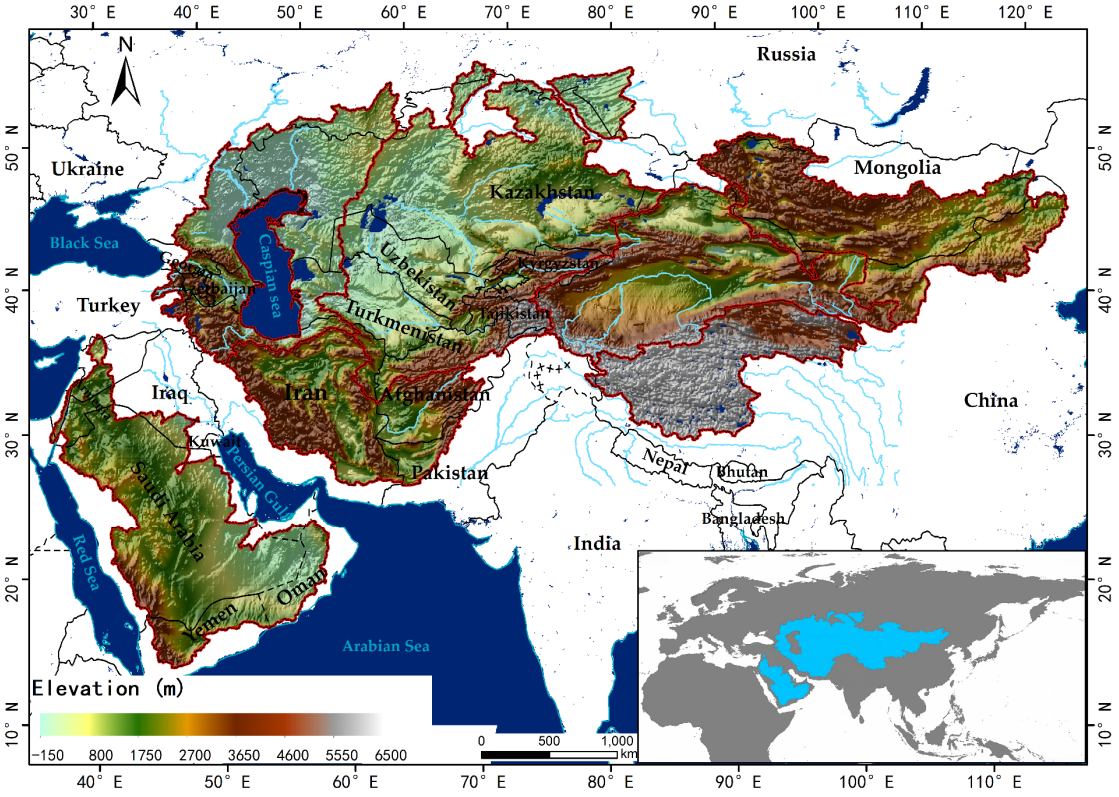

Figure 1. Spatial extent and elevation of the Asian Endorheic Basins (AEB).

We identified our study area based on the map of the Endorheic Basins boundary from the National Tibetan Plateau Science Data Center (http://data.tpdc.ac.cn/en/) and the HydroSHEDS (http://www.hydrosheds.org). A summary of these regions is shown in Table 1.

Table 1. Overview of six inland regions in the AEB.

Basin Name	Area (×10^{4}km^2)	Average Altitude (m)	Aridity Index	TEM (℃)	PRE (mm)	Total Population in 2020 (×10^4)

Centra Asia	339.4	697.8	0.21	8.6	338.3	8781.0
Caspian Sea	159.1	471.5	0.25	10.2	421.3	5425.6
Mongolia Plateau	162.7	1430.0	0.14	4.0	180.8	424.3
Northwest China	169.3	1828.8	0.11	6.7	140.7	2982.9
Qinghai Tibet Plateau	97.5	4551.4	0.16	-3.9	212.7	110.1
Western Asia	317.9	928.0	0.05	22.5	118.3	10076.2
Asian Endorheic Basin	1245.9	1651.3	0.15	8.0	235.4	27800.1

2.2 Land-cover types data

We used the GLC_FCS30 global ecosystem types data which contained 29 types and had a spatial resolution of 30 m (Liu et al., 2021b). The product was generated based on a novel and automatic land-cover monitoring strategy designed to couple continuous land-cover change detection models with dynamic updating algorithms. The continuous time-series surface reflectance from Landsat imagery from 1984 to 2020 and local adaptive modeling were used to produce the global 30-m land-cover dynamic monitoring products. A summary on the area and fraction of each ecosystem type in the study area is shown in Table 2, and the spatial distribution of ecosystem types in 2020 is shown in Figure 2a.

Table 2. Ecosystem types in Asian endorheic basins in 2000 and 2020.

Name	2000		2020	
	Area ($\times 10^4$ km²)	Percentage (%)	Area ($\times 10^4$ km²)	Percentage (%)
Bare areas	746.76	44.30	722.85	42.88
Grassland	317.60	18.84	308.82	18.32
Sparse vegetation	239.97	14.24	249.07	14.77
Shrubland	101.62	6.03	110.93	6.58
Rainfed cropland	141.31	8.38	145.60	8.64
Irrigated cropland	47.77	2.83	48.58	2.88
Forest	40.05	2.38	41.03	2.43
Water body	23.48	1.39	24.61	1.46
Permanent ice/snow	15.12	0.90	16.21	0.96
Impervious surfaces	4.80	0.28	9.09	0.54
Wetlands	7.06	0.42	9.04	0.54

2.3 Aridity index data

To better understand the dependence of vegetation response to hydroclimatic factors, we used an aridity index (AI) to describe the long-term background climate of each pixel obtained from the Global Aridity Index and Potential Evapotranspiration (ETo) Meteorology Database v2 (https://cgiarcsi.community/). AI is defined as:

$$AI = \frac{P}{ET_o} \quad (1)$$

where P is the annual precipitation (mm), and ET0 is the annual average potential evapotranspiration (mm). The P was obtained from the WorldClim2 Global Meteorology Data (https://www.worldclim.org/), while the ET0 was derived from the monthly averaged data in the Global-ETo and further aggregated to generate annual average values (MA-ETo). The aridity zones of the study area based on the AI are presented in Table 3, and Figure 2(d) shows the aridity classes of the study area.

Table 3. Summary of the study area based on aridity index.

AI Value	Aridity Class*	Area ($\times 10^4$ km²)	Percentage (%)
0-0.05	Hyper-arid	309.8	26.5
0.05-0.2	Arid	558.8	47.7
0.2 – 0.5	Semi-arid	264.5	22.6
0.5 – 0.65	Semi-humid	20.7	1.8
> 0.65	Humid	17.2	1.5

* Classification is based on the UNEP (The United Nations Environment Programme, https://www.unep.org/).

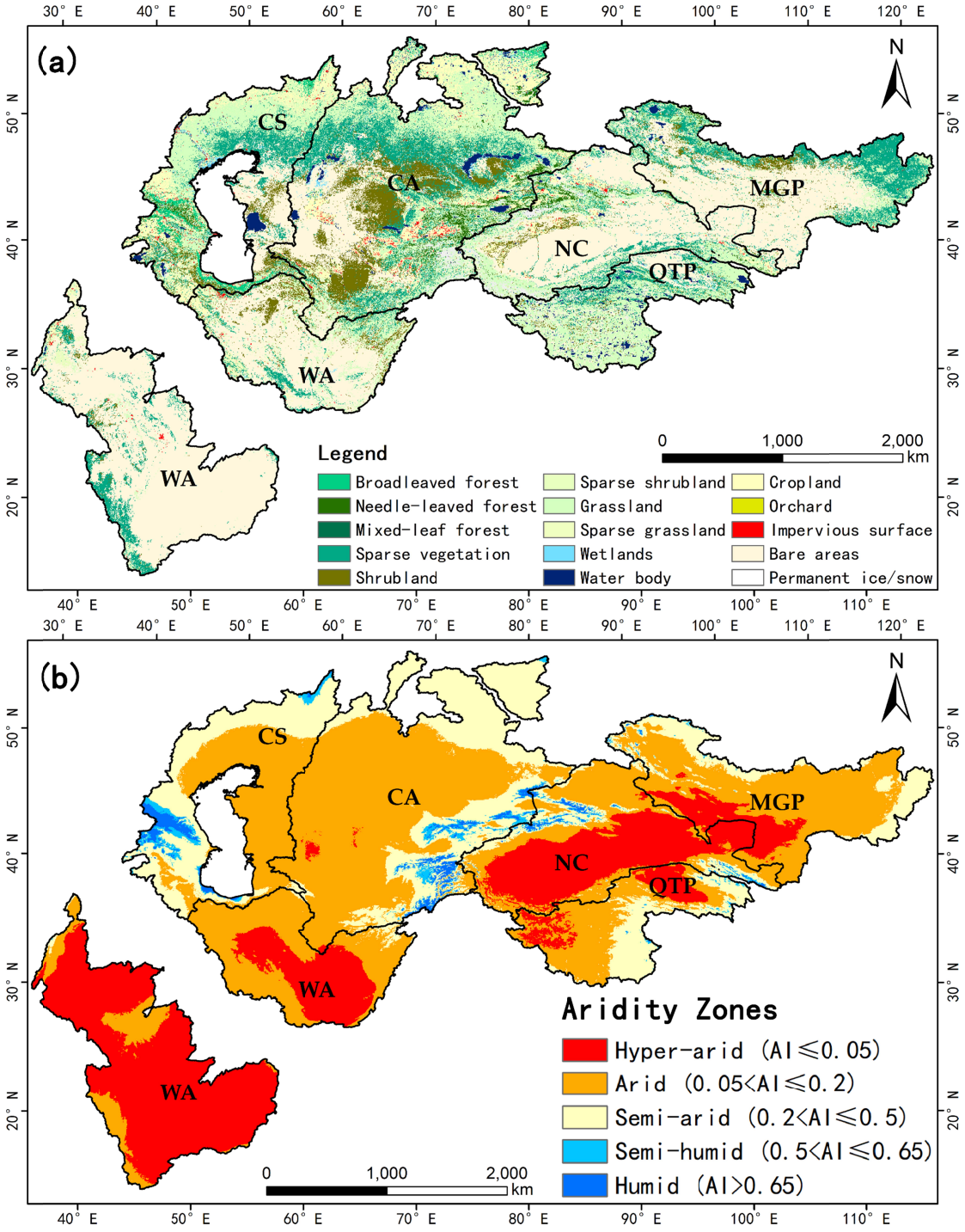

Figure 2. Spatial pattern of ecosystem types (**a**) and aridity zones (**b**). MGP: Mongolia Plateau, QTP: Qinghai Tibet Plateau, NC: Northwest China, CA: Central Asia, CS: Caspian Sea, WA: Western Asia.

2.4 Meteorological data

We obtained ERA5-land monthly average 2-m air temperature data, with a spatial resolution of $0.1° \times 0.1°$, from ECMWF (European Centre for Medium-Range Weather

Forecasts) (https://cds.meteorology.copernicus.eu). ERA5-land is a reanalysis dataset which provides a consistent view of the evolution of land variables over several decades at an enhanced resolution compared to ERA5, providing a reliable record of past climate conditions (Hersbach et al., 2020; Dee et al., 2011).

Global precipitation measurement (GPM) dataset, a monthly precipitation record, was obtained from the NASA GES DISC at NASA Goddard Space Flight Center at a spatial resolution of $0.1° \times 0.1°$ (https://disc.gsfc.nasa.gov/datasets/GPM_3IMERGM_06). The GPM is an international satellite mission designed to provide next-generation observations of rain and snow worldwide. The Integrated Multi-Satellite Retrievals for GPM (IMERG) is the unified algorithm that provides rainfall estimates by interpolating data from all satellite microwave or microwave-corrected infrared precipitation and monthly precipitation gauge records (Huffman et al., 2019a, b). Here we converted the monthly data with the unit of mm/hr into the total precipitation amount during the measurement period. The GPM version 6 record is only available from June 1, 2000, to September 1, 2021, and the missing data from 2021 are filled by using the values of data in the same months from 2016-2020.

2.5 GRACE Total Water Storage Anomalies (TWSA) data

GRACE Total Water Storage Anomalies (TWSA) data were obtained from The Physical Oceanography Distributed Active Archive Center (PODAAC) and processed by Jet Propulsion Laboratory (JPL) (NASA/JPL, 2019). This dataset contains gridded monthly global water storage/height anomalies derived from GRACE and GRACE-FO observations by using the Mascon approach (Version2/RL06). TWSA data are always used for analyzing ocean, ice, and hydrology phenomena, and are provided in equivalent water thickness units (cm) with a spatial resolution of $0.5° \times 0.5°$ (Landerer et al., 2020). The data are available for every month since April 2002 to the present, although there are 33 months with missing data. The averaged values of the same month in the most recent five data-available years were used to fill the gaps. We also used this dataset to calculate the cumulative TWSA, or cTWSA, which represented the long-term departure of TWSA from its "normal" cycle. This approach is widely used for quantitatively estimating the variation of TWSA in response to environmental or anthropogenic interference (Li et al., 2022b). cTWSA is calculated as follows:

$$cTWSA_k = \sum_{i=1}^{k} TWSA_i \tag{2}$$

where k is the kth year of the time series, i is the serial number, i.e. 1-20 from 2002 to 2021.

2.6 MODIS Enhanced Vegetation Index data

The Enhanced Vegetation Index (EVI) is widely used as a proxy of canopy "greenness", which is defined as an integrative composite property of green leaf area, green foliage cover, structure, and leaf chlorophyll content (Huete et al., 2002; Glenn et al., 2008). EVI was developed based on the 1st-order Beer's law application of canopy radiative transfer, optimizing the combination of reflectance in the red, near-infrared (NIR), and blue bands, thus effectively reducing soil background influences and atmospheric noise variations (Huete, 1988; Huete et al., 2002, 2006). EVI is calculated thusly:

$$EVI = 2.5 \times \frac{\rho_{NIR} - \rho_{red}}{\rho_{NIR} + 6\rho_{red} - 7.5\rho_{blue} + 1} \tag{3}$$

where ρ_{NIR}, ρ_{red} and ρ_{blue} are reflectance in the near-infrared, red, and blue bands respectively (Huete et al., 2002). In this study, we opted to use MODIS Collection-6 monthly 0.05° EVI products (MOD13C2) from January 2001 to December 2021 obtained from the USGS repository (ftp://e4ftl01.cr.usgs.gov) to investigate regional vegetation growth patterns. Residual cloud and aerosol contamination in the original EVI time series were filtered out based on the quality assurance (QA) flags provided in the MOD13C2 products, after which the remaining gaps were filled by linear interpolation in the temporal dimension. Additionally, we generated an integrated EVI (hereafter IntEVI) specifically for the annual growing season by summing up the values of EVI from April to October of each year.

$$IntEVI_n = \sum_{i=4}^{10} EVI_{n,i} \quad (4)$$

where *n* and *i* represent the year number and month, separately.

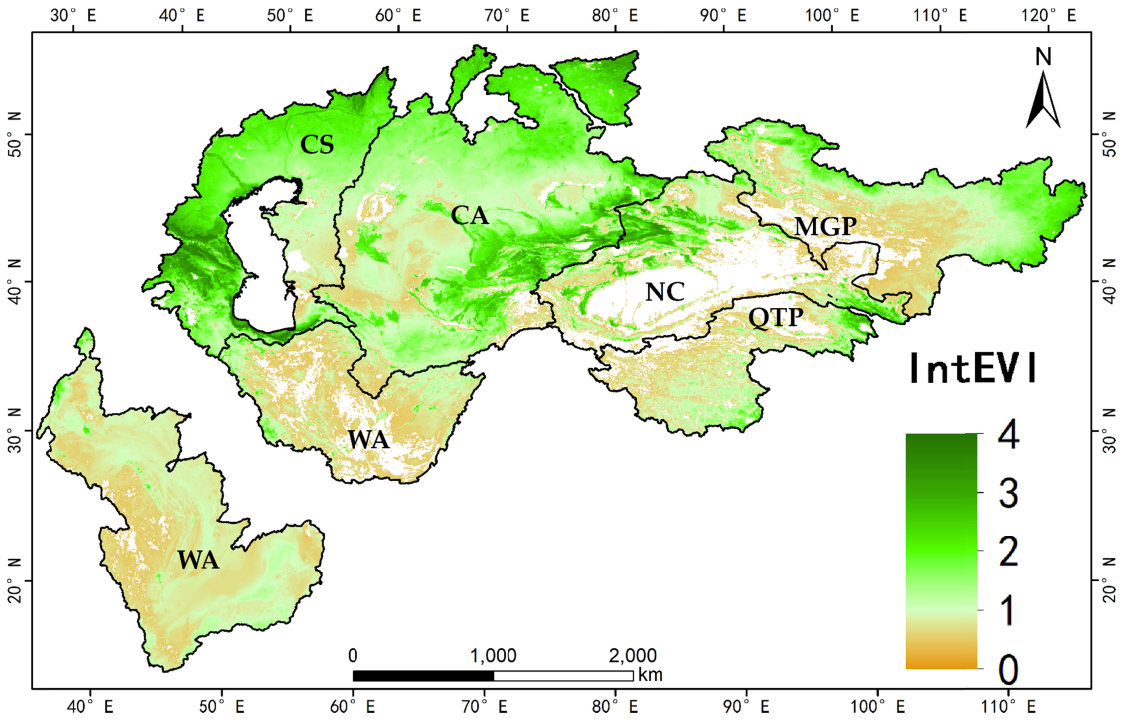

Figure 3 Spatial pattern of average annual IntEVI in AEB from 2001 to 2021.

2.7 Temporal Trend Analysis

Inter-annual changes in IntEVI in the study area from 2001 to 2021 were assessed by the linear trend analysis (Stow et al., 2004; Zhang et al., 2019). The rate of change, or the slope of the linear trend, is calculated as follows:

$$Slope = \frac{n\sum_{i=1}^{n} i \times IntEVI_i - \sum_{i=1}^{n} i \sum_{i=1}^{n} IntEVI_i}{n\sum_{i=1}^{n} i^2 - (\sum_{i=1}^{n} i)^2} \quad (5)$$

We then used an *F* test to test if IntEVI was changing over time (Song et al., 2010). The calculation formulas are as following:

$$F = \frac{r^2(n-2)}{1-r^2} \quad (6)$$

$$r = \frac{\sum_{i=1}^{n}(1-\bar{\imath})(IntEVI_i - \overline{IntEVI})}{\sqrt{\sum_{i=1}^{n}(i-\bar{\imath})^2 \sum_{i=1}^{n}(IntEVI_i - \overline{IntEVI})^2}} \quad (7)$$

where n is 21, and i is the serial number, i.e. 1-21 from 2001 to 2021. $\bar{\imath}$ is the mean value of the serial number, $IntEVI_i$ is the value of IntEVI in the ith year, $\overline{IntEVI}$ is the average IntEVI from 2001 to 2021. When slope > 0% · yr^{-1}, IntEVI shows an increasing trend. When slope < 0% · yr^{-1}, IntEVI shows a decreasing trend. The grading criteria for the trend of IntEVI changes is shown in Table 4.

Table 4. IntEVI changing trend grading criteria (Liu et al., 2020)

IntEVI trend grading criteria	Grade
P-value < 0.05 AND slope $> 0\% \cdot \mathrm{yr}^{-1}$	Significant increase
P-value > 0.05 AND slope $> 0\% \cdot \mathrm{yr}^{-1}$	Slight increase
P-value > 0.05 AND slope $< 0\% \cdot \mathrm{yr}^{-1}$	Slight decrease
P-value < 0.05 AND slope $< 0\% \cdot \mathrm{yr}^{-1}$	Significant decrease

2.8 Partial Correlation Analysis

Partial correlation analysis was used to analyze the relationship between IntEVI change and the changes in any given hydroclimatic variable (Zhao et al., 2015; Ge et al., 2018). By using partial correlation analysis, it is able to remove the obfuscating effects of collinearity in hydroclimatic variables. The partial correlation coefficient of variables x and y when z is fixed is calculated (Du et al., 2020):

$$r_{xy,z} = \frac{r_{xy} - r_{xz}r_{yz}}{\sqrt{(1-r_{xz}^2)(1-r_{yz}^2)}} \quad (8)$$

where $r_{xy,z}$ is the first-order partial correlation coefficient, i is IntEVI, y and z are hydroclimatic factors such as temperature, precipitation, or TWSA. r_{xy}, and both r_{xz}, and r_{yz} are Pearson correlation coefficients.

The coefficient representing the relationship between IntEVI and certain hydroclimatic factors with the other two being fixed was calculated as the second-order partial correlation coefficient ($r_{xy,zw}$) (Xie et al., 2019):

$$r_{xy,zw} = \frac{r_{xy,z} - r_{xw,z}r_{yw,z}}{\sqrt{(1-r_{xw,z}{}^2)+(1-r_{yw,z}{}^2)}} \quad (9)$$

where $r_{xy,z}$, $r_{xw,z}$, and $r_{yw,z}$ represent partial correlations among variables x, y, when controlling variables z and w in the first order.

T test is then used to analyze the relationship between IntEVI and hydroclimatic factors, and the significance test at $p=0.05$ level was conducted in the correlation analysis.

3 Results

3.1 Trends in temperature, precipitation, and TWSA across the AEB over the past two decades

More than 80% of the AEB became increasingly warmer at an average rate of 0.03℃/yr (p<0.05) from 2001 to 2021 (Fig. 4a, Fig. 5a). Although annual precipitation over the entire AEB presented less variation, certain regions had much greater spatial variability in precipitation trend than in temperature (Fig. 4a, Fig. 5b). Northwest China and Western Asia have gradually become wetter, especially in the Hindu Kush Mountains, Aral Sea Basin, and Balkhash Lake, with each having increasingly wetter years at a rate of approximately 10mm/yr (p<0.05)(Fig. 5b). By contrast, Central Asia and the Caspian Sea, especially in the (semi-) humid zones, have gradually become drier at the rate of -5mm/yr (p<0.05) (Fig. 5b).

From 2002 to 2021, 68.64% of the AEB showed a significant decrease in TWSA. The entire region was impacted, and the average TWSA of the AEB decreased at a rate of 0.35 cm/yr (p<0.01) despite maintaining seasonal fluctuations (Fig. 4b). The cumulative TWSA (cTWSA) was -42.2 cm until 2021 (Fig. 4b). Interestingly, several areas, such as the QTP and north of the CA (Fig. 5c) showed the opposite trend with a significant increase in TWSA, although these areas account for less than 17.4 % of the AEB.

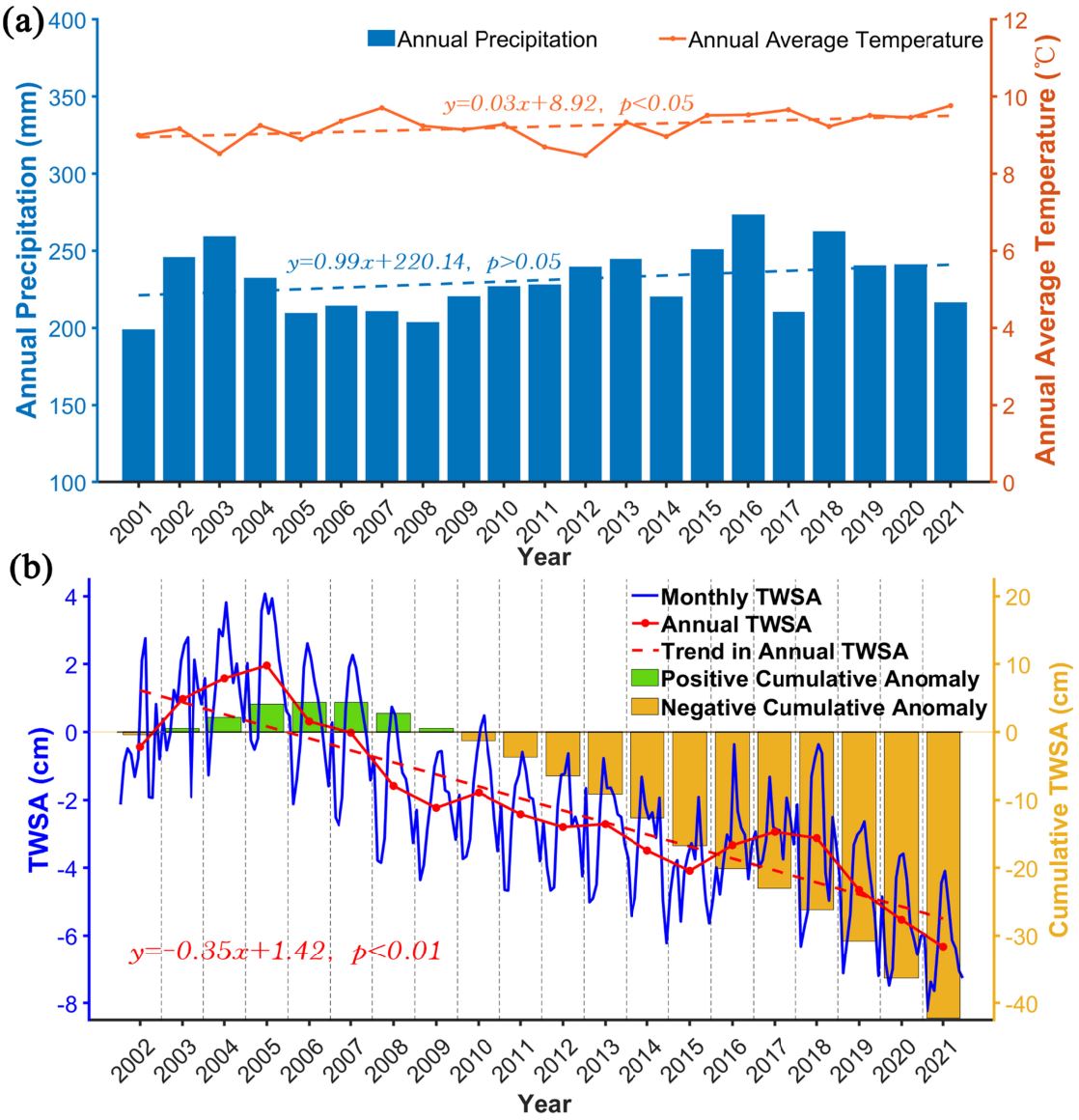

Figure 4. Trends of annual average temperature & total precipitation (**a**) and TWSA (**b**) averaged across the entire AEB during the past two decades.

3.2 Trends of growing season integrated EVI (IntEVI) over the AEB from 2001 to 2021

Annual average growing season integrated EVI (IntEVI, a satellite proxy of vegetation productivity) of the AEB from 2001-2021 is low (with a value of 0.91) though there is high spatial heterogeneity (Fig. 3) consistent with climate classification (Fig. 2d). From 2001 to 2021, the average IntEVI across the entire AEB presented a significant greening trend at a rate of 3.6×10^{-3}/yr. Nearly two-third (65.53%) of the AEB showed a greening trend, of which 34.41% was statistically significant ($p<0.05$) (Fig. 5d). The regions with significant greening trends were marked with red circles in Figure 5(d), in which Northwest China accounting for 13.59% of the AEB by area showed the strongest greening trend at the rate of 7×10^{-3}/yr, or twice the AEB-wide average trend (Fig. 6d). Conversely, Central Asia, Caspian Sea, and the Arabian Peninsula have browned over the last 20 years, accounting for more than 90% of browning across the entire

AEB (Fig. 6d). The northeast of the Caspian Sea Basin, the middle of the Arabian Peninsula, and the Yili River Valley in the Northwest China, which had the most significant browning trends, are marked with blue circles in Fig. 5d.

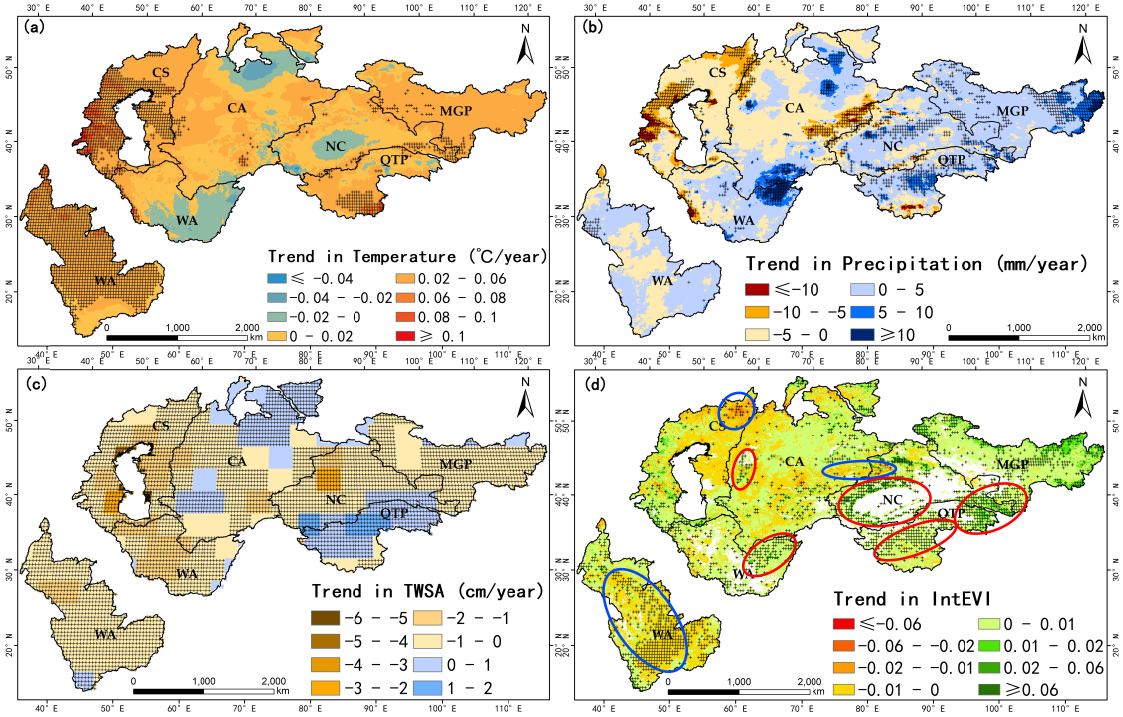

Figure 5. Spatial distribution of the trends in annual average temperature (**a**), total precipitation (**b**), TWSA (**c**), and IntEVI (**d**) in the Asian endorheic basins (2001–2021). The black crosses (+) indicate areas with a statistically significant ($p < 0.05$) trend (same as below). The circles in (**d**) are typical regions selected with significant greening (blue) and browning (red) trend, respectively.

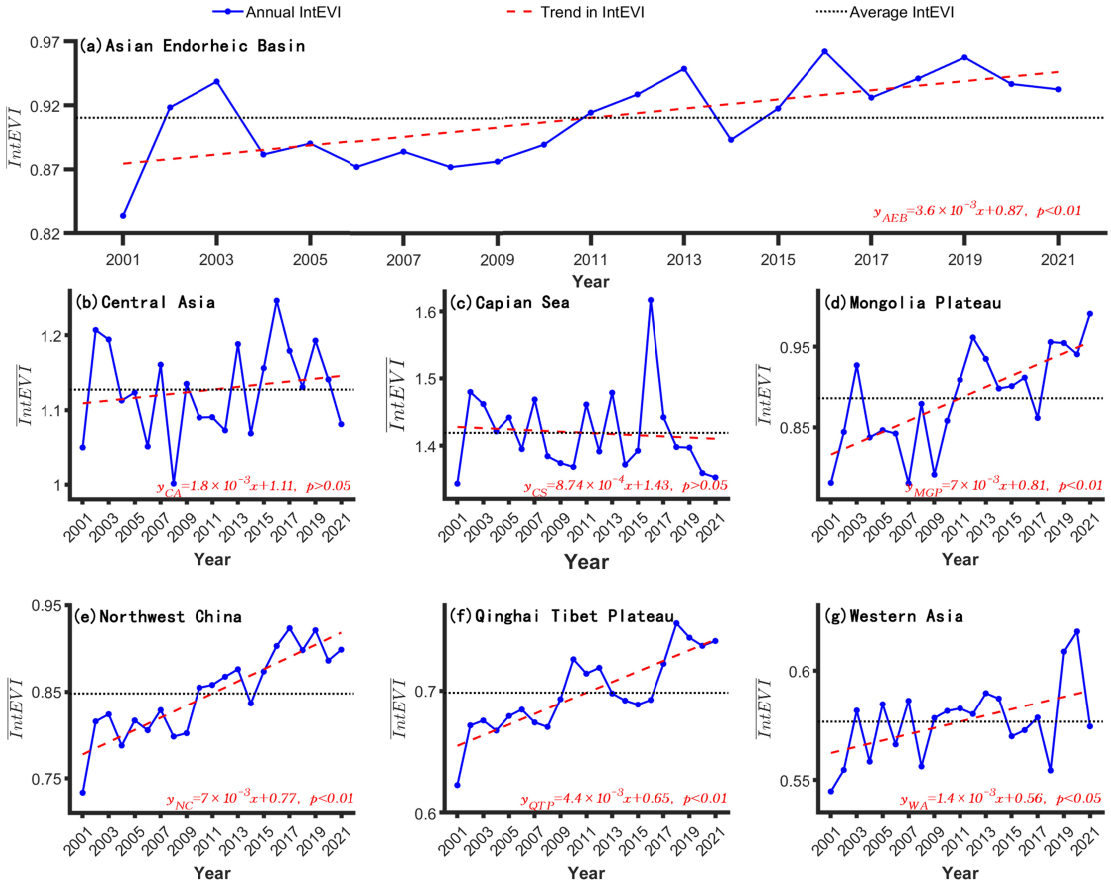

Figure 6. The trends of IntEVI averaged across Central Asia (CA), Caspian Sea (CS), Mongolia Plateau (MGP), Northwest China (NC), Qinghai Tibet Plateau (QTP) and Western Asia (WA) from 2001 to 2021.

We observed that most greening happened in arid and hyper-arid regions (Fig. 7). Furthermore, among land cover types, irrigated cropland exhibited the largest IntEVI trend, followed by rainfed cropland and shrubland (Fig. 7). By contrast, all land cover types in semi-arid and (semi)-humid regions exhibited a non-significant trend in IntEVI.

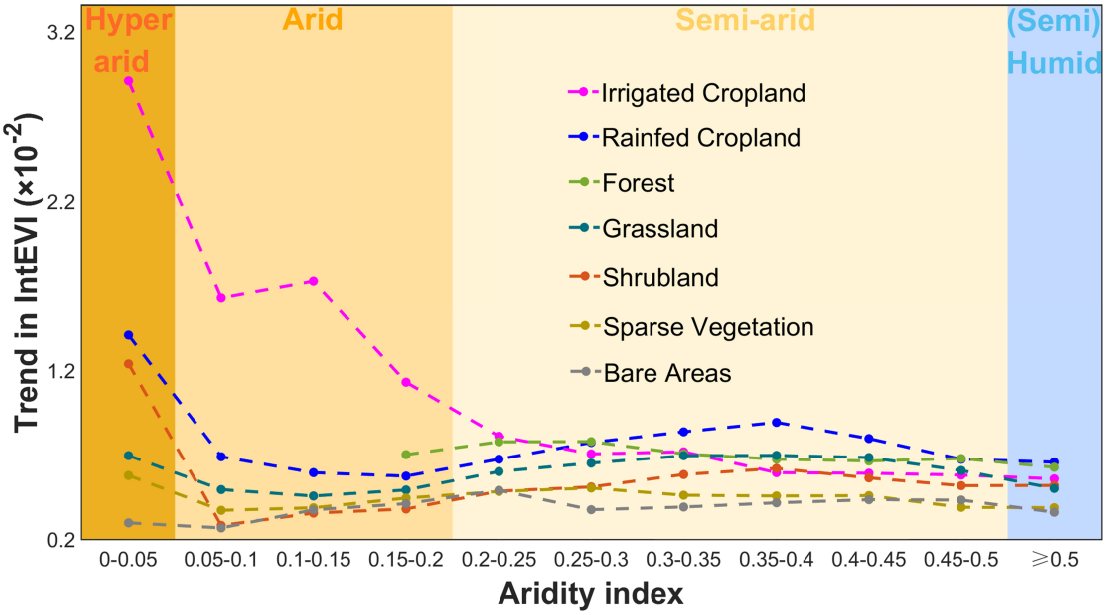

Figure 7. The trend of IntEVI from 2001 to 2021 for the major land cover types averaged across the aridity index bins in the study area. Pixels' values of IntEVI trend (linear slope) over the entire study area are averaged by bin (every 0.05 increment) of aridity index.

3.3 Relative importance of temperature, precipitation, and TWSA in driving IntEVI trend

Both positive and negative correlations between IntEVI and temperature were observed (Fig. 8a), while the correlation between IntEVI and precipitation was more prevailingly positive over the study area (Fig. 8b). Contrasting correlations were found between IntEVI and TWSA in the Northwest China (Tianshan Mountains and Altai Mountains) and Qinghai-Tibet Plateau (including Kunlun Mountains) (Fig. 8c). Additionally, negative correlations were also found in the Iran Plateau and Middle of the Mongolia Plateau, while the other zones totally presented positive correlations (Fig. 8c).

The relative importance of temperature, precipitation, and TWSA in driving IntEVI change was mapped using the RGB plot (Fig. 8d). It indicates that the change in IntEVI across half of the study area can be explained mainly by changes in precipitation from 2001-2021, while only 2% of change is caused primarily by temperature (Fig. 8d). The remaining area was almost equally controlled by temperature, precipitation and TWSA. IntEVI trend in about 17% of areas is mainly associated with the TWSA change, largely found in Northwest China, Qinghai Tibet Plateau and Arabian Peninsula (Fig. 8d).

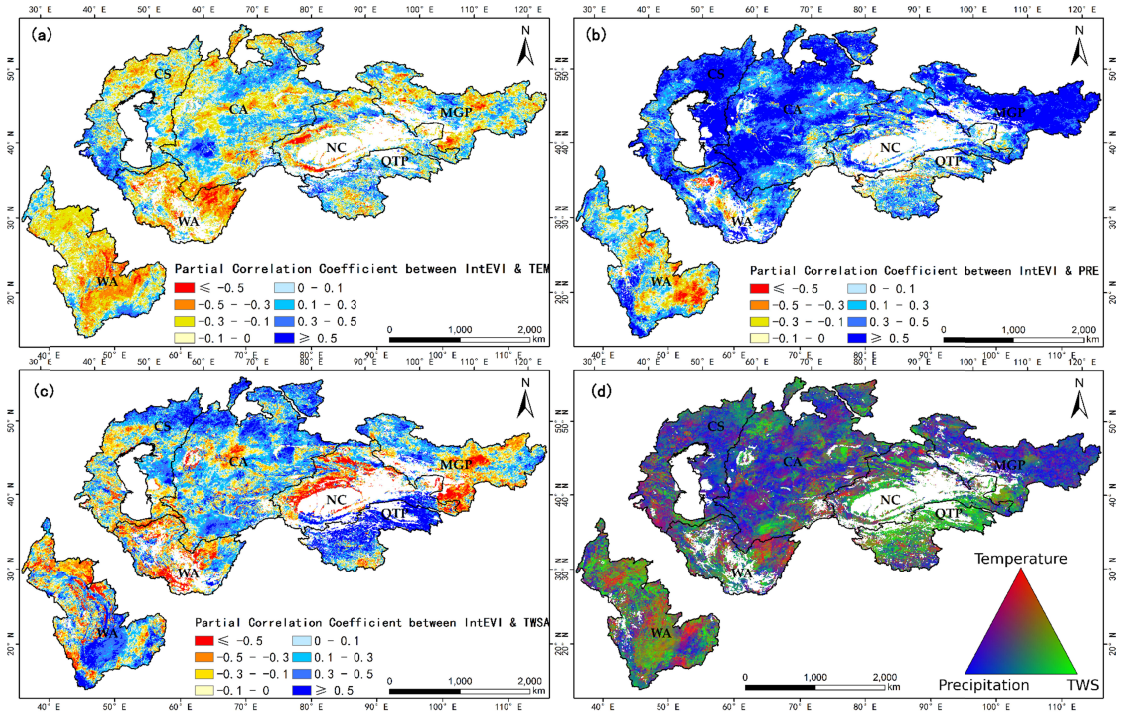

Figure 8. Partial correlation coefficient between IntEVI and temperature (**a**), precipitation (**b**), and TWSA (**c**) from 2002 to 2021. (**d**) Distribution of the relative importance among three hydroclimatic factors to vegetation productivity trend across Asian endorheic basins with red representing the temperature dominant zone, blue indicating the precipitation dominant zone, and green representing the TWS dominant zone.

The relative importance of temperature, precipitation, and GRACE TWSA varied across the aridity gradient. Precipitation played a dominant role in driving the vegetation productivity trend across almost the entire aridity gradient and such dominance increased with the increase in aridity. However, the dominance of precipitation gave way to TWSA as soon as moving into the hyper-arid region, which can be interpreted as a decoupling of rainfall and vegetation productivity trend and a switch from the dependence to atmospheric water to groundwater.

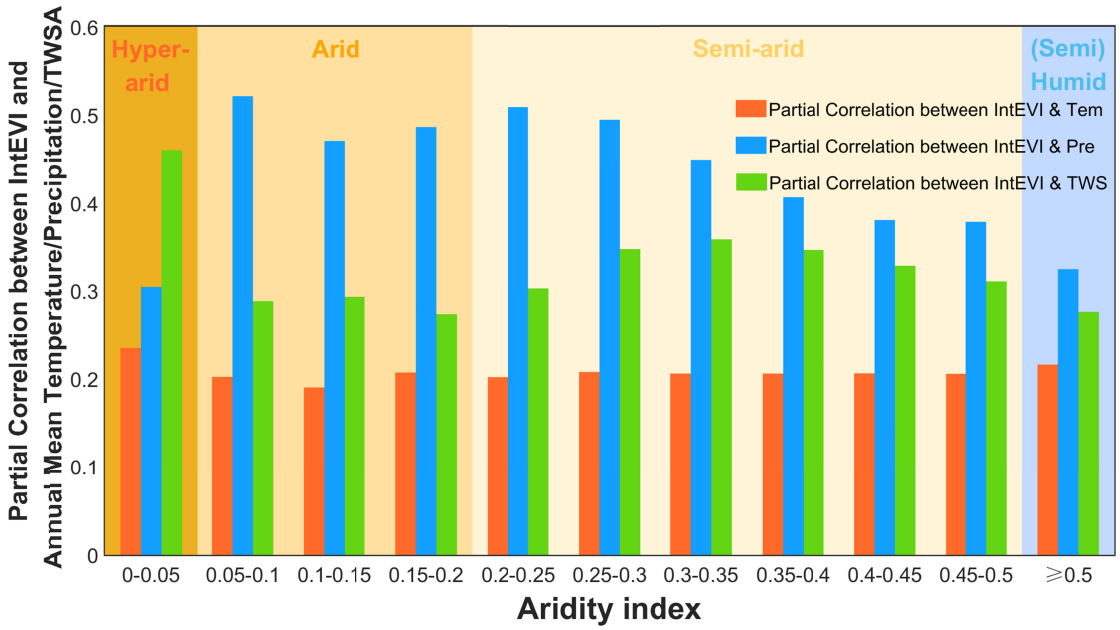

Figure 9. Partial correlation coefficients between IntEVI and temperature (orange bars), precipitation (blue bars), and TWSA (green bars) aggregated by aridity index bins in the study area. The partial correlation coefficients over the entire study area are averaged by bin (every 0.05 or 0.5 increments) of the aridity index.

The significant vegetation greening in hyper-arid AEB was quite unusual and the decoupling of such trend to rainfall was also very intriguing. To decipher the underlying driving forces, we analyzed the changes in land cover types in different aridity zones across the AEB. Our results indicated that there was a significant, 17.3%- and 4.3%-fold increase in the area of irrigated cropland in the arid and hyper-arid AEB. By contrast, there was a significant, 2.6%- and 18.0%-fold decrease in the area of irrigated cropland in the semi-arid and (semi-) humid AEB (Fig. 10). Putting together several lines of evidences, the observed greening in hyper-arid AEB can be mainly attributed to the expansion of the irrigated cropland and such an intensified use of groundwater can further explain the dramatic decline in TWSA leading to decoupling of vegetation productivity and rainfall in such dry and harsh environment.

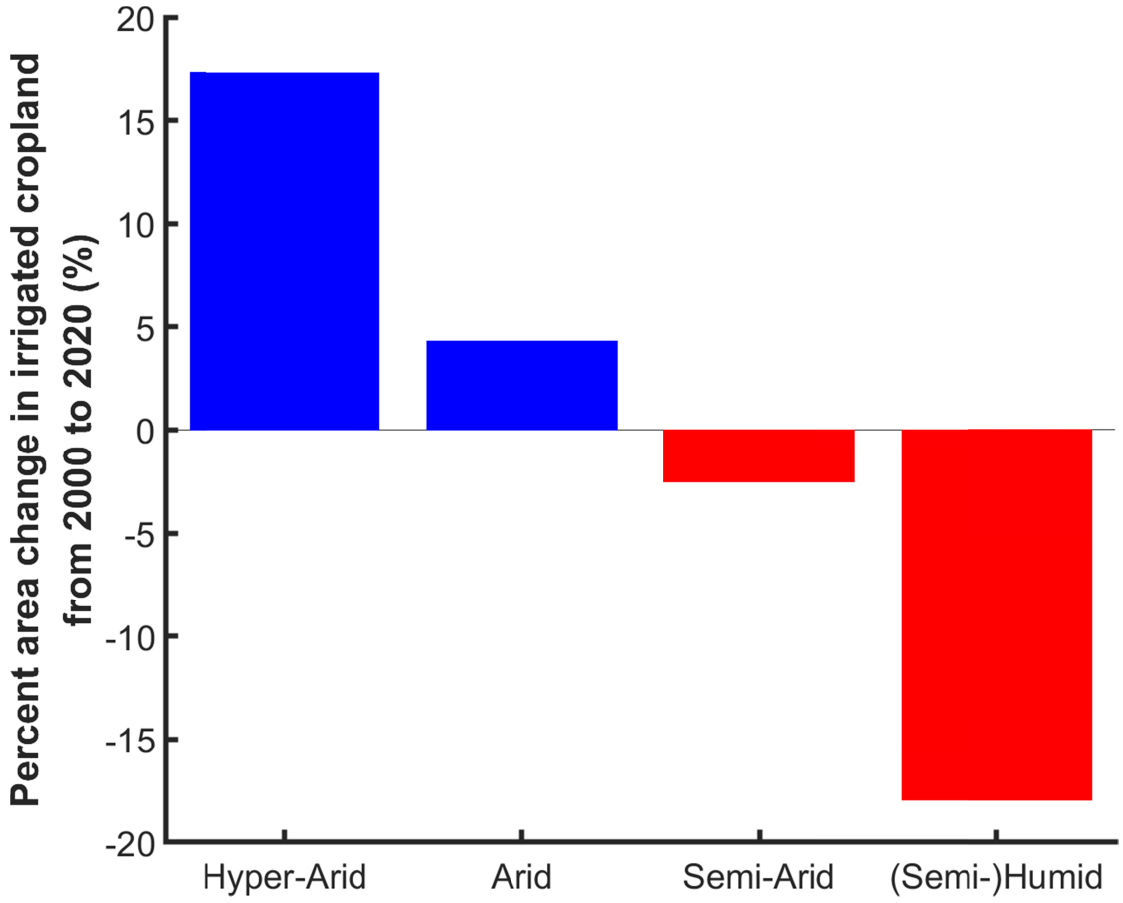

Figure 10. Percent area change in irrigated cropland from 2000 to 2020.

4 Discussion

4.1 Vegetation trend in the AEB from 2001 to 2021 as revealed by MODIS EVI

This study showed that MODIS IntEVI averaged across the entire AEB increased significantly during the 2001-2021 period, indicating an overall greening phenomenon. This is in agreement with the recent studies reporting widespread vegetation greening in temperate arid regions worldwide (Cortés et al., 2021; Fensholt et al., 2012; Piao et al., 2020).

Despite this consistency, we present our research to emphasize the heterogeneous spatial distribution of vegetation greening, and perhaps more importantly, the varying driving forces of the apparent greening trend in different regions. The AEB is a diverse and highly variable region, and it has seen similarly variable change over the last two decades. Similar to the previous studies, Mongolia Plateau, Northwest China, Qinghai Tibet Plateau, and Western Asia exhibited the most significant greening phenomena (Ghorbanian et al., 2022; Zhao et al., 2022; Zhang et al., 2023), and were responsible for more than 90% of the greening trend of the entire AEB, respectively. In contrast, both Central Asia, Caspian Sea, and the Arabian Peninsula showed oscillating trends of browning and greening which ultimately accounted for less than 10% of the AEB greening (Lewinska et al., 2020; Xu et al., 2016).

Reviewing the impacts of land cover type on vegetation change, we found that irrigated cropland 'greened-up' the most over the last 20 years, particularly in hyper-arid zones, and likely represented oases cultivation efforts in basins and their surrounding regions (such as Tarim River Basin in the southern Tianshan Mountains). We also found the same directional trend in a few scattered areas in some mountainous regions (such as Hindu Kush Mountains), consistent with results from Ma et al. (2019) and Zhao et al. (2022), albeit these changes were less pronounced than those observed in oases. Similarly, greening trends were observed in the oases of Northwest China perhaps due to the creation of artificial oases as a means of agricultural development (Ma et al., 2019; Ning et al., 2021).

While previous studies have suggested that vegetation has degraded in Central Asia and the Caspian Sea, our study did not confirm this as we only observed a fluctuating IntEVI, at least within the past two decades (Hao et al., 2022; Li et al., 2015; Xu et al., 2016). We speculate that the discrepancy between our results and the previous ones can be attributed to several reasons. One possible explanation is the difference in sampling data. Previous studies mainly used the GIMMS3g NDVI from NOAA/AVHRR sensors to detect vegetation trends during 1982-2015 (Du et al., 2019; Du et al., 2020; Li et al., 2015; Yuan et al., 2021; Yuan et al., 2022), while in this study, we used the better calibrated MODIS vegetation indices products to analyze the trend from 2001-2021. Vegetation in Central Asia and the Caspian Sea had indeed experienced accelerating greening to browning reversals since 1994 (Pan et al., 2018), however, in the late 1990s, this degradation gradually slowed down and stalled especially in northern mid-latitude (Yin et al., 2016). As we excluded data during that period of degradation, our results did not include the browning observed in the mid 1990's. Similarly, our results may be skewed spatially. For example, in this study, Kazakhskiy Melkosopochnik (KM), where grassland covered more than 70% of the areas and was also found to be the severest degradation region in Central Asia (Li et al., 2015; Xu et al., 2016), was excluded from the AEB, which likely masked a large proportion of browning (Dubovyk et al., 2016; Liu et al., 2021a).

4.2 Potential factors driving widespread greening trend in the AEB

It is reasonable to expect that water, represented in both input (precipitation) and loss (evapotranspiration), is a major factor influencing the large-scale patterns of vegetation growth in the AEB. Precipitation is the major and direct water supply of soil moisture in the AEB (Wang et al., 2020), and unsurprisingly the relationship between IntEVI and precipitation showed an overall highly positive correlation (Fig. 8b, Fig. 9). However, we also found an interesting TWSA-driven pattern, especially the contrasting and dominant impact in Northwest China and Qinghai Tibet Plateau. According to the land surface water balance equation, TWSA variation is mainly influenced by hydroclimatic and anthropogenic water consumption. Therefore, TWSA may be considered an integrative indicator of the water cycle (Pan et al., 2017), drought/soil moisture (Pokhrel et al., 2021), and human activity intensity (An et al., 2021).

The change in irrigated cropland indicated that human irrigated agriculture has intensified by 17.3% and 4.3% in hyper-arid and arid zones (Fig. 10), respectively, during the past two decades. Irrigated cropland has expanded by more than 58% since the 1990s (Fu et al., 2022), furthermore, a previous study suggested that approximately 70% of the increase in actual evapotranspiration was attributed to increased river diversions for irrigation from groundwater and glacial melt runoff, and this human disturbance is captured by changes in TWSA (Liu, 2022). With consideration of our results, this may indicate that human water consumption in the

driest zones during the past several decades likely induces a more severe water scarcity in the future, ultimately forming a vicious negative feedback loop. Our results imply that this speculation could explain the observed sensitivity of vegetation in the Caucasus region and the Aral Sea Basin to TWSA, given both their history of agricultural development and "hot-dry" climate change (Dehghanipour et al., 2020; Ghale et al., 2018; Yang et al., 2021).

Human change, however, is not all negative. Revegetation and restoration programs also likely contributed to the greening trend as we observed across the region. For example, the Chinese government has implemented many ecological restoration projects in Northwest China (Cao et al., 2020; Viña et al., 2016; Wang et al., 2014; Yuan et al., 2014). These projects have positive effects on the local environment (Dong et al., 2019; Wang et al., 2022; Yu et al., 2022) and their contributions to the observed greening trend are revealed in this study (Fig. 5c-d). However, it is worth noting that revegetation and ecological restoration projects also artificially change the water supply-demand relationship (Cao et al., 2022), and in arid regions such as the AEB, especially where precipitation is the single water supply, these restoration projects may need to refocus, and re-prioritize sustainable constraints imposed by the regional water availability, now and in the future (Du et al., 2021).

4.3 Limitations and future perspectives

From the data perspective, the 2-m air temperature data derived from the ERA-5 reanalysis dataset is a derivative product generated by combining model data with observations from all sites across the world (Hersbach et al., 2020). Data quality is thus determined by the number and the representativeness of weather stations. The potential to generalize this data is highly variable, and depends on a host of factors, including topography. Meanwhile, due to the coarse spatial resolution (0.5°), GRACE-TWSA pixels at the junction of basins, especially basins with small areas, may actually cover different natural geographical units. For example, pixels in the southern Tarim River Basin cover parts of the Kunlun Mountains, which doesn't belong to this basin (Fig. 5c).

We integrated the MOD13C2 EVI from the growing season as the indicator of vegetation productivity. Other vegetation parameters such as LAI and GPP were also adopted to analyze global vegetation characteristics and the response to climate change (Piao et al., 2014; Zhu et al., 2016). Although these vegetation indices and parameters showed a consistent trend, discrepancies were also observed (Zeng et al., 2022). Hence, results from the IntEVI may be corroborated by other satellite proxies and field plots from the long-term ecological networks to confirm the ecosystem productivity change (Guadagno et al., 2017). In addition, besides temperature, precipitation, and terrestrial water storage we selected, vegetation change could also be affected by a variety of other global change factors such as CO_2 fertilization and nitrogen deposition (e.g., Zhu et al. 2016), which were not considered in this study.

Despite these limitations, this study still offers valuable insight into how vegetation has changed over the last two decades in the AEB. These results, and our generalized observations on the relation between climate, land cover type, aridity, and human development can guide large-scale ecological restorations and sustainable plans to address the challenges of future climate change in an extremely vulnerable environment. Future work should focus on establishing long-term ground observations covering a large spatial gradient to confirm the vegetation changes detected through satellite products (Piao et al., 2020). In addition, further remote sensing to gather complementary data should be considered, such as aboveground

biomass (AGB) derived from the GEDI spaceborne LiDAR mission and the Solar induced chlorophyll fluorescence (SIF) derived from TanSat or OCO-2/3 spaceborne missions (Pan et al., 2018).

5 Conclusions

In this study, we assessed the spatio-temporal vegetation variation trends encompassing the key Asian endorheic basins during 2001-2021 using MODIS EVI. Furthermore, we analyzed the relationship between vegetation change and a suite of hydroclimatic variables using second-order partial correlation analysis. The results revealed an overall greening trend across the AEB, though we observed extreme spatial heterogeneity. The greening trend was most pronounced in Northwest China, Qinghai Tibet Plateau, and Western Asia. Interestingly, we found that while precipitation had the dominant control effect in arid and semi-arid zones, vegetation change in hyper-arid zones was most closely associated with water storage anomalies. Additionally, we found that a significant expansion of irrigated cropland in (hyper-) arid zones was positively correlated with greening, suggesting that some fraction of greening can be attributed to hyper-arid agricultural development (such as oases cultivation). This study highlights the decisive impact of hydroclimate conditions modulated by human activities on vegetation growth in the arid and hyper-arid areas within the AEB, hence can guide the management of the fragile dryland ecosystems by establishing sustainability constraints to agriculture expansion in the future.

Acknowledgments

This study is supported by General Program National Natural Science Foundation of China (No. 42171305, Principal Investigator: X. Ma); NSFC Projects of International Cooperation and Exchanges (No. 42311540014, PI: X. Ma); Natural Science Foundation of Gansu Province, China (No. 21JR7RA499, PI: X. Ma); Director Fund of the International Research Center of Big Data for Sustainable Development Goals (No. CBAS2022DF006, PI: X. Ma); Fundamental Research Funds for the Central Universities (No. lzujbky-2021-ct11, PI: X. Ma).

Open Research

All the data that support this study can be freely accessed using the websites or data repositories described below. The border shapefile of the AEB is extracted from the National Tibetan Plateau Science Data Center (https://data.tpdc.ac.cn/zh-hans/data/34060a43-f30e-4b06-8265-025c8b6aae99) and the HydroSHEDS (https://www.hydrosheds.org/products/hydrobasins). The 30-m resolution global land cover types dataset in 2020 is available at the CAS Earth Data Sharing and Service Portal (https://data.casearth.cn/sdo/detail/5fbc7904819aec1ea2dd7061). The aridity index data is available at the Global Aridity Index and Potential Evapotranspiration (ETo) Meteorology Database v2 (https://figshare.com/articles/dataset/Global_Aridity_Index_and_Potential_Evapotranspiration_ET0_Climate_Database_v2/7504448/3). The 2-m monthly air temperature data is available at the ECMWF provided by GEE platform (https://developers.google.com/earth-engine/datasets/catalog/ECMWF_ERA5_LAND_MONTHLY_AGGR). The precipitation data is available at the NASA GES DISC at NASA Goddard Space Flight Center (https://disc.gsfc.nasa.gov/datasets/GPM_3IMERGM_06). The terrestrial water storage normalies data is available at the PODAAC

(https://podaac.jpl.nasa.gov/dataset/TELLUS_GRAC-GRFO_MASCON_CRI_GRID_RL06_V2). And the EVI data of MOD13C2 product is available at LP DAAC (https://lpdaac.usgs.gov/products/mod13c2v006/). All the analyses and plots were conducted using the MATLAB's framework for statistical computing, available via https://ww2.mathworks.cn/products/matlab.html (Version R2021a). All the maps were drew using the ArcGIS Desktop's framework, available via https://www.esri.com/en-us/arcgis/products/index (Version 10.4).

My data are textual—the information and ideas contained in the references listed below. Where links for articles exist, I have provided them. I have not provided library links for books.

References

1. Alizade Govarchin Ghale, Y., Altunkaynak, A., & Unal, A. (2017). Investigation Anthropogenic Impacts and Climate Factors on Drying up of Urmia Lake using Water Budget and Drought Analysis. *Water Resources Management*, 32(1), 325-337. https://doi.org/10.1007/s11269-017-1812-5
2. An, L., Wang, J., Huang, J., Pokhrel, Y., Hugonnet, R., Wada, Y., Cáceres, D., Müller Schmied, H., Song, C., Berthier, E., Yu, H., & Zhang, G. (2021). Divergent Causes of Terrestrial Water Storage Decline Between Drylands and Humid Regions Globally. *Geophysical Research Letters*, 48(23). https://doi.org/10.1029/2021gl095035
3. Cao, Y., Kong, L., Zhang, L., & Ouyang, Z. (2020). Spatial characteristics of ecological degradation and restoration in China from 2000 to 2015 using remote sensing. *Restoration Ecology*, 28(6), 1419-1430. https://doi.org/10.1111/rec.13226
4. Cao, Y., Xie, Z., Woodgate, W., Ma, X., Cleverly, J., Pang, Y., Qin, F., & Huete, A. (2022). Ecohydrological decoupling of water storage and vegetation attributed to China's large-scale ecological restoration programs. *Journal of Hydrology*, 615. https://doi.org/10.1016/j.jhydrol.2022.128651
5. Center for International Earth Science Information Network - CIESIN - Columbia University. (2018). Gridded Population of the World, Version 4 (GPWv4): Population Count, Revision 11 NASA Socioeconomic Data and Applications Center (SEDAC). https://doi.org/10.7927/H4JW8BX5
6. Chen, Y., Chen, L., Cheng, Y., Ju, W., Chen, H. Y. H., & Ruan, H. (2020). Afforestation promotes the enhancement of forest LAI and NPP in China. *Forest Ecology and Management*, 462. https://doi.org/10.1016/j.foreco.2020.117990
7. Cortés, J., Mahecha, M. D., Reichstein, M., Myneni, R. B., Chen, C., & Brenning, A. (2021). Where Are Global Vegetation Greening and Browning Trends Significant? *Geophysical Research Letters*, 48(6). https://doi.org/10.1029/2020gl091496
8. Dehghanipour, A. H., Moshir Panahi, D., Mousavi, H., Kalantari, Z., & Tajrishy, M. (2020). Effects of Water Level Decline in Lake Urmia, Iran, on Local Climate Conditions. *Water*, 12(8). https://doi.org/10.3390/w12082153
9. Dee, D. P., Uppala, S. M., Simmons, A. J., Berrisford, P., Poli, P., Kobayashi, S., Andrae, U., Balmaseda, M. A., Balsamo, G., Bauer, P., Bechtold, P., Beljaars, A. C. M., van de Berg, L., Bidlot, J., Bormann, N., Delsol, C., Dragani, R., Fuentes, M., Geer, A. J., . . . Vitart, F. (2011). The ERA-Interim reanalysis: configuration and performance of the data assimilation system. *Quarterly Journal of the Royal Meteorological Society*, 137(656), 553-597. https://doi.org/10.1002/qj.828
10. Ding, Z., Peng, J., Qiu, S., & Zhao, Y. (2020). Nearly Half of Global Vegetated Area

539 Experienced Inconsistent Vegetation Growth in Terms of Greenness, Cover, and
540 Productivity. *Earth's Future*, 8(10). https://doi.org/10.1029/2020ef001618
541 11. Dong, S.-k., Sha, W., Su, X.-k., Zhang, Y., Li, S., Gao, X., Liu, S.-l., Shi, J.-b., Liu, Q.-r., &
542 Hao, Y. (2019). The impacts of geographic, soil and climatic factors on plant diversity,
543 biomass and their relationships of the alpine dry ecosystems: Cases from the Aerjin
544 Mountain Nature Reserve, China. *Ecological Engineering*, 127, 170-177.
545 https://doi.org/10.1016/j.ecoleng.2018.10.027
546 12. Du, J., Quan, Z., Fang, S., Liu, C., Wu, J., & Fu, Q. (2020). Spatiotemporal changes in
547 vegetation coverage and its causes in China since the Chinese economic reform.
548 *Environment Science and Pollution Research*, 27(1), 1144-1159.
549 https://doi.org/10.1007/s11356-019-06609-6
550 13. Du, L., Zeng, Y., Ma, L., Qiao, C., Wu, H., Su, Z., & Bao, G. (2021). Effects of
551 anthropogenic revegetation on the water and carbon cycles of a desert steppe ecosystem.
552 *Agricultural and Forest Meteorology*, 300. https://doi.org/10.1016/j.agrformet.2021.108339
553 14. Du, Z., Zhao, J., Pan, H., Wu, Z., & Zhang, H. (2019). Responses of vegetation activity to
554 the daytime and nighttime warming in Northwest China. *Environment Monitoring and*
555 *Assessment*, 191(12), 721. https://doi.org/10.1007/s10661-019-7855-8
556 15. Dubovyk, O., Landmann, T., Dietz, A., & Menz, G. (2016). Quantifying the Impacts of
557 Environmental Factors on Vegetation Dynamics over Climatic and Management Gradients
558 of Central Asia. *Remote Sensing*, 8(7). https://doi.org/10.3390/rs8070600
559 16. Fensholt, R., Langanke, T., Rasmussen, K., Reenberg, A., Prince, S. D., Tucker, C., Scholes,
560 R. J., Le, Q. B., Bondeau, A., Eastman, R., Epstein, H., Gaughan, A. E., Hellden, U., Mbow,
561 C., Olsson, L., Paruelo, J., Schweitzer, C., Seaquist, J., & Wessels, K. (2012). Greenness in
562 semi-arid areas across the globe 1981–2007 — an Earth Observing Satellite based analysis
563 of trends and drivers. *Remote Sensing of Environment*, 121, 144-158.
564 https://doi.org/10.1016/j.rse.2012.01.017
565 17. Fu, J., Wang, W., Zaitchik, B., Nie, W., Fei, E. X., Miller, S. M., & Harman, C. J. (2022).
566 Critical Role of Irrigation Efficiency for Cropland Expansion in Western China Arid
567 Agroecosystems. *Earth's Future*, 10(9). https://doi.org/10.1029/2022ef002955
568 18. Ge, J., Meng, B., Liang, T., Feng, Q., Gao, J., Yang, S., Huang, X., & Xie, H. (2018).
569 Modeling alpine grassland cover based on MODIS data and support vector machine
570 regression in the headwater region of the Huanghe River, China. *Remote Sensing of*
571 *Environment*, 218, 162-173. https://doi.org/10.1016/j.rse.2018.09.019
572 19. Guadagno, C. R., Ewers, B. E., Speckman, H. N., Aston, T. L., Huhn, B. J., DeVore, S. B.,
573 Ladwig, J. T., Strawn, R. N., & Weinig, C. (2017). Dead or Alive? Using Membrane Failure
574 and Chlorophyll a Fluorescence to Predict Plant Mortality from Drought. *Plant Physiology*,
575 175(1), 223-234. https://doi.org/10.1104/pp.16.00581
576 20. Ghorbanian, A., Mohammadzadeh, A., & Jamali, S. (2022). Linear and Non-Linear
577 Vegetation Trend Analysis throughout Iran Using Two Decades of MODIS NDVI Imagery.
578 *Remote Sensing*, 14(15). https://doi.org/10.3390/rs14153683
579 21. Glenn, E. P., Huete, A. R., Nagler, P. L., & Nelson, S. G. (2008). Relationship Between
580 Remotely-sensed Vegetation Indices, Canopy Attributes and Plant Physiological Processes
581 What Vegetation Indices Can and Cannot Tell Us About the Landscape. *Sensors*, 8, 2136-
582 2160. https://doi.org/10.3390/s8042136
583 22. Hao, H., Chen, Y., Xu, J., Li, Z., Li, Y., & Kayumba, P. M. (2022). Water Deficit May
584 Cause Vegetation Browning in Central Asia. *Remote Sensing*, 14(11).

https://doi.org/10.3390/rs14112574

23. He, H., Luo, G., Cai, P., Hamdi, R., Termonia, P., De Maeyer, P., Kurban, A., & Li, J. (2021). Assessment of Climate Change in Central Asia from 1980 to 2100 Using the Köppen-Geiger Climate Classification. *Atmosphere*, 12(1). https://doi.org/10.3390/atmos12010123
24. Hersbach, H., Bell, B., Berrisford, P., Hirahara, S., Horányi, A., Muñoz-Sabater, J., Nicolas, J., Peubey, C., Radu, R., Schepers, D., Simmons, A., Soci, C., Abdalla, S., Abellan, X., Balsamo, G., Bechtold, P., Biavati, G., Bidlot, J., Bonavita, M., . . . Thépaut, J. N. (2020). The ERA5 global reanalysis. *Quarterly Journal of the Royal Meteorological Society*, 146(730), 1999-2049. https://doi.org/10.1002/qj.3803
25. Huang, L., He, B., Chen, A., Wang, H., Liu, J., Lu, A., & Chen, Z. (2016). Corrigendum: Drought dominates the interannual variability in global terrestrial net primary production by controlling semi-arid ecosystems. *Scientific Reports*, 6, 35126. https://doi.org/10.1038/srep35126
26. Huang, M., Piao, S., Ciais, P., Penuelas, J., Wang, X., Keenan, T. F., Peng, S., Berry, J. A., Wang, K., Mao, J., Alkama, R., Cescatti, A., Cuntz, M., De Deurwaerder, H., Gao, M., He, Y., Liu, Y., Luo, Y., Myneni, R. B., . . . Janssens, I. A. (2019). Air temperature optima of vegetation productivity across global biomes. *Nature Ecology & Evolution*, 3(5), 772-779. https://doi.org/10.1038/s41559-019-0838-x
27. Huete A. (1988). A Soil-Adjusted Vegetation Index (SAVI). *Remote Sensing of Environment*, 25, 295-309. https://doi.org/10.1016/0034-4257(88)90106-X
28. Huete, A., Didan, K., Miura, T., Rodriguez, E., Gao, X., & Ferreira, L. (2002). Overview of the radiometric and biophysical performance of the MODIS vegetation indices. *Remote Sensing of Environment*, 83, 195-213. https://doi.org/0034-4257
29. Huete, A. R., Didan, K., Shimabukuro, Y. E., Ratana, P., Saleska, S. R., Hutyra, L. R., Yang, W., Nemani, R. R., & Myneni, R. (2006). Amazon rainforests green-up with sunlight in dry season. *Geophysical Research Letters*, 33(6). https://doi.org/10.1029/2005gl025583
30. Huffman, G.J., Bolvin, D.T., Braithwaite, D., Hsu, K., Joyce, R., Kidd, C., Nelkin, E.J.,Sorooshian, S., Tan, J., Xie, P., 2019a. Algorithm Theoretical Basis Document(ATBD) Version 06, NASA Global Precipitation Measurement (GPM) Integrated MultisatellitE Retrievals for GPM (IMERG), National Aeronautics and Space Administration (NASA).
31. Huffman, G.J., Bolvin, D.T., Nelkin, E.J., Tan, J., 2019b. Integrated Multi-satellitE Retrievals for GPM (IMERG) Technical Documentation, *IMERG Tech Document*,National Aeronautics and Space Administration (NASA).
32. Jiang, Y., Wang, R., Peng, Q., Wu, X., Ning, H., & Li, C. (2018). The relationship between drought activity and vegetation cover in Northwest China from 1982 to 2013. *Natural Hazards*, 92(S1), 145-163. https://doi.org/10.1007/s11069-018-3282-3
33. Jiao, L., Wang, X., Cai, D., & Hua, T. (2021). Potential responses of vegetation to atmospheric aerosols in arid and semi-arid regions of Asia. *Journal of Arid Land*, 13(5), 516-533. https://doi.org/10.1007/s40333-021-0005-5
34. Landerer, F. W., Flechtner, F. M., Save, H., Webb, F. H., Bandikova, T., Bertiger, W. I., Bettadpur, S. V., Byun, S. H., Dahle, C., Dobslaw, H., Fahnestock, E., Harvey, N., Kang, Z., Kruizinga, G. L. H., Loomis, B. D., McCullough, C., Murböck, M., Nagel, P., Paik, M., . . . Yuan, D. N. (2020). Extending the Global Mass Change Data Record: GRACE Follow-On Instrument and Science Data Performance. *Geophysical Research Letters*, 47(12). https://doi.org/10.1029/2020gl088306

35. Lewińska, K. E., Hostert, P., Buchner, J., Bleyhl, B., & Radeloff, V. C. (2020). Short-term vegetation loss versus decadal degradation of grasslands in the Caucasus based on Cumulative Endmember Fractions. *Remote Sensing of Environment*, 248. https://doi.org/10.1016/j.rse.2020.111969
36. Li, Z., Chen, Y., Li, W., Deng, H., & Fang, G. (2015). Potential impacts of climate change on vegetation dynamics in Central Asia. *Journal of Geophysical Research: Atmospheres*, 120(24), 12345-12356. https://doi.org/10.1002/2015jd023618
37. Liang, Y., Liu, L., & Hashimoto, S. (2020). Spatiotemporal analysis of trends in vegetation change across an artificial desert oasis, Northwest China, 1975–2010. *Arabian Journal of Geosciences*, 13(15). https://doi.org/10.1007/s12517-020-05707-x
38. Liu, C., Li, W., Zhu, G., Zhou, H., Yan, H., & Xue, P. (2020). Land Use/Land Cover Changes and Their Driving Factors in the Northeastern Tibetan Plateau Based on Geographical Detectors and Google Earth Engine: A Case Study in Gannan Prefecture. *Remote Sensing*, 12(19). https://doi.org/10.3390/rs12193139
39. Liu, C., Yan, X., & Jiang, F. (2021a). Desert vegetation responses to the temporal distribution patterns of precipitation across the northern Xinjiang, China. *Catena*, 206. https://doi.org/10.1016/j.catena.2021.105544
40. Liu, L., Zhang, X., Gao, Y., Chen, X., Shuai, X., & Mi, J. (2021b). Finer-Resolution Mapping of Global Land Cover: Recent Developments, Consistency Analysis, and Prospects. *Journal of Remote Sensing*, 2021, 1-38. https://doi.org/10.34133/2021/5289697
41. Liu, Y., Chen, Y., & Ge, L. (2018). Analysis on exploitation status, potential and strategy of groundwater resources in the five countries of Central Asia. *Journal of Groundwater Science and Engineering*, 6, 49-57. https://doi.org/10.19637/j.cnki.2305-7068.2018.01.006
42. Liu, Z. (2022). Causes of changes in actual evapotranspiration and terrestrial water storage over the Asian inland basins. *Hydrological Processes*, 36(1). https://doi.org/10.1002/hyp.14482
43. Luo, M., Sa, C., Meng, F., Duan, Y., Liu, T., & Bao, Y. (2020). Assessing extreme climatic changes on a monthly scale and their implications for vegetation in Central Asia. *Journal of Cleaner Production*, 271. https://doi.org/10.1016/j.jclepro.2020.122396
44. Ma, L., Yang, S., Gu, Q., Li, J., Yang, X., Wang, J., & Ding, J. (2019). Spatial and temporal mapping of cropland expansion in northwestern China with multisource remotely sensed data. *Catena*, 183. https://doi.org/10.1016/j.catena.2019.104192
45. Mander, L., Dekker, S. C., Li, M., Mio, W., Punyasena, S. W., & Lenton, T. M. (2017). A morphometric analysis of vegetation patterns in dryland ecosystems. *Royal Society Open Science*, 4(2), 160443. https://doi.org/10.1098/rsos.160443
46. Mohamed, A. H., & Squires, V. R. (2018). Drylands of the Mediterranean Basin: Challenges, Problems and Prospects. *In Climate Variability Impacts on Land Use and Livelihoods in Drylands* (pp. 223-239). https://doi.org/10.1007/978-3-319-56681-8_11
47. Mu, L., Fang, L., Dou, W., Wang, C., Qu, X., & Yu, Y. (2021). Urbanization-induced spatio-temporal variation of water resources utilization in northwestern China: A spatial panel model based approach. *Ecological Indicators*, 125. https://doi.org/10.1016/j.ecolind.2021.107457
48. Na, R., Na, L., Du, H., He, H. S., Shan, Y., Zong, S., Huang, L., Yang, Y., & Wu, Z. (2021). Vegetation Greenness Variations and Response to Climate Change in the Arid and Semi-Arid Transition Zone of the Mongo-Lian Plateau during 1982–2015. *Remote Sensing*, 13(20). https://doi.org/10.3390/rs13204066

49. Nagler, P. L., Glenn, E. P., Kim, H., Emmerich, W., Scott, R. L., Huxman, T. E., & Huete, A. R. (2007). Relationship between evapotranspiration and precipitation pulses in a semiarid rangeland estimated by moisture flux towers and MODIS vegetation indices. *Journal of Arid Environments*, 70(3), 443-462. https://doi.org/10.1016/j.jaridenv.2006.12.026
50. Nasa/Jpl. (2019). JPL GRACE and GRACE-FO Mascon Ocean, Ice, and Hydrology Equivalent Water Height Coastal Resolution Improvement (CRI) Filtered Release 06 Version 02 NASA Physical Oceanography DAAC. https://doi.org/10.5067/TEMSC-3JC62
51. Ning, J. (2021). Effects of Cropland Expansion on the Regional Land Surface Radiative Energy Balance and Heat Fluxes in Northern China. *Applied Sciences*, 11(4). https://doi.org/10.3390/app11041556
52. Pan, Y., Zhang, C., Gong, H., Yeh, P. J. F., Shen, Y., Guo, Y., Huang, Z., & Li, X. (2017). Detection of human-induced evapotranspiration using GRACE satellite observations in the Haihe River basin of China. *Geophysical Research Letters*, 44(1), 190-199. https://doi.org/10.1002/2016gl071287
53. Pan, N., Feng, X., Fu, B., Wang, S., Ji, F., & Pan, S. (2018). Increasing global vegetation browning hidden in overall vegetation greening: Insights from time-varying trends. *Remote Sensing of Environment*, 214, 59-72. https://doi.org/10.1016/j.rse.2018.05.018
54. Piao, S., Nan, H., Huntingford, C., Ciais, P., Friedlingstein, P., Sitch, S., Peng, S., Ahlstrom, A., Canadell, J. G., Cong, N., Levis, S., Levy, P. E., Liu, L., Lomas, M. R., Mao, J., Myneni, R. B., Peylin, P., Poulter, B., Shi, X., . . . Chen, A. (2014). Evidence for a weakening relationship between interannual temperature variability and northern vegetation activity. *Nature Communications*, 5, 5018. https://doi.org/10.1038/ncomms6018
55. Piao, S., Wang, X., Park, T., Chen, C., Lian, X., He, Y., Bjerke, J. W., Chen, A., Ciais, P., Tømmervik, H., Nemani, R. R., & Myneni, R. B. (2020). Characteristics, drivers and feedbacks of global greening. *Nature Reviews Earth & Environment*, 1(1), 14-27. https://doi.org/10.1038/s43017-019-0001-x
56. Pokhrel, Y., Felfelani, F., Satoh, Y., Boulange, J., Burek, P., Gädeke, A., Gerten, D., Gosling, S. N., Grillakis, M., Gudmundsson, L., Hanasaki, N., Kim, H., Koutroulis, A., Liu, J., Papadimitriou, L., Schewe, J., Müller Schmied, H., Stacke, T., Telteu, C.-E., . . . Wada, Y. (2021). Global terrestrial water storage and drought severity under climate change. *Nature Climate Change*, 11(3), 226-233. https://doi.org/10.1038/s41558-020-00972-w
57. Riis, T., Kelly-Quinn, M., Aguiar, F. C., Manolaki, P., Bruno, D., Bejarano, M. D., Clerici, N., Fernandes, M. R., Franco, J. C., Pettit, N., Portela, A. P., Tammeorg, O., Tammeorg, P., Rodríguez-González, P. M., & Dufour, S. (2020). Global Overview of Ecosystem Services Provided by Riparian Vegetation. *BioScience*, 70(6), 501-514. https://doi.org/10.1093/biosci/biaa041
58. Safriel, U., & Adeel, Z. (2008). Development paths of drylands: thresholds and sustainability. *Sustainability Science*, 3(1), 117-123. https://doi.org/10.1007/s11625-007-0038-5
59. Seka, A. M., Zhang, J., Prodhan, F. A., Ayele, G. T., Finsa, M. M., Sharma, T. P. P., & Melesse, A. M. (2022). Hydrological drought impacts on water storage variations: a focus on the role of vegetation changes in the East Africa region. A systematic review. *Environment Science Pollution Researth*, 29(53), 80237-80256. https://doi.org/10.1007/s11356-022-23313-0
60. Shang, J., Zhang, Y., Peng, Y., Huang, Y., Zhu, L., Wu, Z., Wang, J., & Cui, Y. (2022). Climate change drives NDVI variations at multiple spatiotemporal levels rather than human

disturbance in Northwest China. *Environment Science Pollution Researth*, 29(10), 13782-13796. https://doi.org/10.1007/s11356-021-16774-2

61. Smith, W. K., Dannenberg, M. P., Yan, D., Herrmann, S., Barnes, M. L., Barron-Gafford, G. A., Biederman, J. A., Ferrenberg, S., Fox, A. M., Hudson, A., Knowles, J. F., MacBean, N., Moore, D. J. P., Nagler, P. L., Reed, S. C., Rutherford, W. A., Scott, R. L., Wang, X., & Yang, J. (2019). Remote sensing of dryland ecosystem structure and function: Progress, challenges, and opportunities. *Remote Sensing of Environment*, 233. https://doi.org/10.1016/j.rse.2019.111401
62. Song, Y., Ma, M., & Veroustraete, F. (2010). Comparison and conversion of AVHRR GIMMS and SPOT VEGETATION NDVI data in China. *International Journal of Remote Sensing*, 31(9), 2377-2392. https://doi.org/10.1080/01431160903002409
63. Stow, D. A., Hope, A., McGuire, D., Verbyla, D., Gamon, J., Huemmrich, F., Houston, S., Racine, C., Sturm, M., Tape, K., Hinzman, L., Yoshikawa, K., Tweedie, C., Noyle, B., Silapaswan, C., Douglas, D., Griffith, B., Jia, G., Epstein, H., . . . Myneni, R. (2004). Remote sensing of vegetation and land-cover change in Arctic Tundra Ecosystems. *Remote Sensing of Environment*, 89(3), 281-308. https://doi.org/10.1016/j.rse.2003.10.018
64. Ukkola, A. M., De Kauwe, M. G., Roderick, M. L., Burrell, A., Lehmann, P., & Pitman, A. J. (2021). Annual precipitation explains variability in dryland vegetation greenness globally but not locally. *Glob Chang Biol*, 27(18), 4367-4380. https://doi.org/10.1111/gcb.15729
65. Vina, A., McConnell, W. J. Y., Hongbo, Xu, Z., & Liu, J. (2016). Effects of conservation policy on China's forest recovery. *Science Advances*, 2(3). https://doi.org/10.1126/sciadv.1500965
66. Wang, Q., Zhang, B., Zhang, Z., Zhang, X., & Dai, S. (2014). The Three-North Shelterbelt Program and Dynamic Changes in Vegetation Cover. *Journal of Resources and Ecology*, 5(1), 53-59. https://doi.org/10.5814/j.issn.1674-764x.2014.01.006
67. Wang, R., Peng, Q., Zhang, W., Zhao, W., Liu, C., & Zhou, L. (2022). Ecohydrological Service Characteristics of Qilian Mountain Ecosystem in the Next 30 Years Based on Scenario Simulation. *Sustainability*, 14(3). https://doi.org/10.3390/su14031819
68. Wang, S., Liu, Q., & Huang, C. (2021). Vegetation Change and Its Response to Climate Extremes in the Arid Region of Northwest China. *Remote Sensing*, 13(7). https://doi.org/10.3390/rs13071230
69. Wang, W., Li, H., Wang, J., & Hao, X. (2020). Water Vapor from Western Eurasia Promotes Precipitation during the Snow Season in Northern Xinjiang, a Typical Arid Region in Central Asia. *Water*, 12(1). https://doi.org/10.3390/w12010141
70. Wei, F., Wang, S., Brandt, M., Fu, B., Meadows, M. E., Wang, L., Wang, L., Tong, X., & Fensholt, R. (2021). Responses and feedbacks of African dryland ecosystems to environmental changes. *Current Opinion in Environmental Sustainability*, 48, 29-35. https://doi.org/10.1016/j.cosust.2020.09.004
71. Xie, Z., Huete, A., Cleverly, J., Phinn, S., McDonald-Madden, E., Cao, Y., & Qin, F. (2019). Multi-climate mode interactions drive hydrological and vegetation responses to hydroclimatic extremes in Australia. *Remote Sensing of Environment*, 231. https://doi.org/10.1016/j.rse.2019.111270
72. Xing, X., Qian, J., Chen, X., Chen, C., Sun, J., Wei, S., Yimamaidi, D., & Zhanar, Z. (2022). Analysis of Effects of Recent Changes in Hydrothermal Conditions on Vegetation in Central Asia. *Land*, 11(3). https://doi.org/10.3390/land11030327
73. Xu, H., Wang, X., & Zhang, X. (2016). Decreased vegetation growth in response to summer

drought in Central Asia from 2000 to 2012. *International Journal of Applied Earth Observation and Geoinformation*, 52, 390-402. https://doi.org/10.1016/j.jag.2016.07.010

74. Xu, Y., Xu, X., & Tang, Q. (2016). Human activity intensity of land surface: Concept, methods and application in China. *Journal of Geographical Sciences*, 26(9), 1349-1361. https://doi.org/10.1007/s11442-016-1331-y
75. Yang, J., Zhang, Q., Lu, G., Liu, X., Wang, Y., Wang, D., Liu, W., Yue, P., Zhu, B., & Duan, X. (2021). Climate Transition from Warm-Dry to Warm-Wet in Eastern Northwest China. *Atmosphere*, 12(5). https://doi.org/10.3390/atmos12050548
76. Yang, X., Wang, N., Chen, A. a., Li, Z., Liang, Q., & Zhang, Y. (2022). Impacts of Climate Change, Glacier Mass Loss and Human Activities on Spatiotemporal Variations in Terrestrial Water Storage of the Qaidam Basin, China. *Remote Sensing*, 14(9). https://doi.org/10.3390/rs14092186
77. Yin, G., Hu, Z., Chen, X., & Tiyip, T. (2016). Vegetation dynamics and its response to climate change in Central Asia. *Journal of Arid Land*, 8(3), 375-388. https://doi.org/10.1007/s40333-016-0043-6
78. Yu, H. (2016). Motivation behind China's 'One Belt, One Road' Initiatives and Establishment of the Asian Infrastructure Investment Bank. *Journal of Contemporary China*, 26(105), 353-368. https://doi.org/10.1080/10670564.2016.1245894
79. Yu, X., Lei, J., & Gao, X. (2022). An over review of desertification in Xinjiang, Northwest China. Journal of Arid Land, 14(11), 1181-1195. https://doi.org/10.1007/s40333-022-0077-x
80. Yuan, W., Li, X., Liang, S., Cui, X., Dong, W., Liu, S., Xia, J., Chen, Y., Liu, D., & Zhu, W. (2014). Characterization of locations and extents of afforestation from the Grain for Green Project in China. *Remote Sensing Letters*, 5(3), 221-229. https://doi.org/10.1080/2150704X.2014.894655
81. Yuan, Y., Bao, A., Jiang, P., Hamdi, R., Termonia, P., De Maeyer, P., Guo, H., Zheng, G., Yu, T., & Prishchepov, A. V. (2022). Probabilistic assessment of vegetation vulnerability to drought stress in Central Asia. *Journal of Environment Management*, 310, 114504. https://doi.org/10.1016/j.jenvman.2022.114504
82. Yuan, Y., Bao, A., Liu, T., Zheng, G., Jiang, L., Guo, H., Jiang, P., Yu, T., & De Maeyer, P. (2021). Assessing vegetation stability to climate variability in Central Asia. *Journal of Environment Management*, 298, 113330. https://doi.org/10.1016/j.jenvman.2021.113330
83. Zeng, X., Hu, Z., Chen, A., Yuan, W., Hou, G., Han, D., Liang, M., Di, K., Cao, R., & Luo, D. (2022). The global decline in the sensitivity of vegetation productivity to precipitation from 2001 to 2018. *Global Change Biology*, 28(22), 6823-6833. https://doi.org/10.1111/gcb.16403
84. Zhang, A., Jia, G., & Ustin, S. L. (2021). Water availability surpasses warmth in controlling global vegetation trends in recent decade: revealed by satellite time series. *Environmental Research Letters*, 16(7). https://doi.org/10.1088/1748-9326/ac0b68
85. Zhang, H., Zhan, C., Xia, J., & Yeh, P. J. (2022). Responses of vegetation to changes in terrestrial water storage and temperature in global mountainous regions. *Sci Total Environ*, 851(Pt 2), 158416. https://doi.org/10.1016/j.scitotenv.2022.158416
86. Zhang, M., Wang, J., & Li, S. (2019). Tempo-spatial changes and main anthropogenic influence factors of vegetation fractional coverage in a large-scale opencast coal mine area from 1992 to 2015. *Journal of Cleaner Production*, 232, 940-952. https://doi.org/10.1016/j.jclepro.2019.05.334
87. Zhang, Z., Ding, J., Zhao, W., Liu, Y., & Pereira, P. (2023). The impact of the armed

conflict in Afghanistan on vegetation dynamics. *Science of the Total Environment*, 856(Pt 2), 159138. https://doi.org/10.1016/j.scitotenv.2022.159138

88. Zhao, Q., Wu, W., & Wu, Y. (2015). Variations in China's terrestrial water storage over the past decade using GRACE data. *Geodesy and Geodynamics*, 6(3), 187-193. https://doi.org/10.1016/j.geog.2015.03.004
89. Zhao, R., Liu, X., Dong, J., Zhao, G., Manevski, K., Andersen, M. N., & Tang, Q. (2022). Human activities modulate greening patterns: a case study for southern Xinjiang in China based on long time series analysis. *Environmental Research Letters*, 17(4). https://doi.org/10.1088/1748-9326/ac58a9
90. Zhu, Z., Piao, S., Myneni, R. B., Huang, M., Zeng, Z., Canadell, J. G., Ciais, P., Sitch, S., Friedlingstein, P., Arneth, A., Cao, C., Cheng, L., Kato, E., Koven, C., Li, Y., Lian, X., Liu, Y., Liu, R., Mao, J., . . . Zeng, N. (2016). Greening of the Earth and its drivers. *Nature Climate Change*, 6(8), 791-795. https://doi.org/10.1038/nclimate3004